Electric Power Components and Systems, 00:000–000, 2018

0731-356X / 18 $12.00 + .00

Optimization of DC Starters Based on Reluctance Network Accounting for Armature Reaction Magnetic Field

Sara BAZHAR[1,2], Julien FONTCHASTAGNER[1]
Noureddine TAKORABET[1], Nicolas LABBE[2]
Raphaël ANDREUX[2]

[1]Université de Lorraine, GREEN
54500 Vandœuvre-lès-Nancy, France
[2]Valeo Electrical Systems
38070 Saint-Quentin-Fallavier, France.

In the new generation of "Stop & Start" starters, a DC series motor with high power density is used. In this application, non symmetrical machines are used due to the single wave winding in brushed motors. The saturation of the iron core in this application reaches a really high level. Moreover armature reaction in DC machine with a large stator pole spans makes this phenomenon even more enhanced. All these criteria lead to model the whole machine in highly saturated conditions which is time consuming. In this paper, a fast reluctance network model for an equivalent machine is proposed. It takes into account the armature reaction in high saturation conditions. It also allows a good accuracy and permits to show the relevance of taking into account this phenomenon in torque calculation. This model is validated by finite element method in many operating points, and by a statistical approach. It shows high robustness and low computation time. Finally, an optimization procedure using this reluctance network model and FE is presented in order to show the accuracy of the RN compared to FE model.

1 Introduction

In "Stop & Start" applications, the used DC machine should have a longer lifetime in comparison with conventional starters. Some authors concluded that the lifetime of the machine is directly related to the brush wear that is affected by current commutation [1, 2], and others suggest to increase the torque produced by the starter to overcome the problems related to the switching [3]. The torque density could be increased through an optimization based on a multiphysical model such as magnetic model coupled with thermal [4, 5] or electrical aspects. Saving CPU time for the magnetic modelling is necessary to take into account all these different phenomena.

This article deals with a magnetic model with reduced CPU time and acceptable accuracy. Several authors have developed models for optimization in the literature. Mahmoudi *et al* [6] proposed an optimization coupled directly with tridimensional

Manuscript received in final form on XXXX XX, 2017.
Address correspondence to J. Fontchastagner.

finite element (3D FE) which is not adapted when considering an important number of variables. Andreux *et al* [3] take into account 3D effects in an equivalent 2D finite element model by including corrector factors in geometrical parameters and in equivalent permeability of the material. This fast and accurate model is developed to optimize the machine but still time consuming compared to analytical models. Other authors propose some analytical models that can predict the distribution of the magnetic potential vector (MVP) in the airgap by solving the Laplace's equation [7,8]. These models are used in an optimization process for an early pre-design stage because of their advantageous CPU time but still limited when it needs to consider the saturation of magnetic material. Although, nonlinear aspects should be taken into account in the design of the motor. For synchronous machines, reluctance network models are developed since a long time [9]. Several authors used this kind of networks to model a claw pole alternator [10, 11], while others [12] considered iron saturation and armature reaction to be coupled with an equivalent electrical model, and it is still used by many authors to model many other types of machines [13–19]. Basically each machine is modeled by a reluctance network. However in an optimization process, each topology change (slot number, pole number) needs to re-built a new network. Nowadays, this approach is developed through a reluctance networks distribution [20], however it makes the model more complex and increase the variable number and CPU time which makes this method similar to the finite element methods. RN models are rarely used for DC machines which are non-symmetrical and need the modeling of the whole machine instead of one period. Moreover, in the starter application, the DC machine is subjected to high level saturation what highlight the effect of armature magnetic reaction (AMR). Labbe *et al* [21] studied the effects of this phenomenon upon the torque, while Li *et al* [22] present the impact of AMR on claw pole alternator in automotive application under high saturation level.

In this paper, a reluctance network for a DC machine is developed and modeling of this non symmetrical topologies with an equivalent symmetrical machine is discussed in order to make the model less complex. Moreover, the consideration of the armature reaction in the modeling of these kinds of machines is highlighted thanks to the torque calculation under highly saturated condition. Saliency effect and flux leakage are taken into account for a good modeling of linkage flux of the machine. The proposed reluctance network model is validated through a statistical approach which consists in generating randomized machines and comparing with results provided by a special 2D finite element accounting for 3D effects [3]. The statistical way to measure the robustness of the model is then presented. The reduced CPU time of the model allows using it in an optimization process on two examples. Generally, the optimization using reluctance network is performed in an early pre-design stage which requires to use finite element to get an optimized result. The model presented here shows the possibility to optimize the motor without needing a further step using finite element model.

2 Magnetic Network modeling of DC Motor

2.1 General Principle

In automotive applications, starting the combustion engine spends few seconds. Generally the efficiency of the machine is not important in this kind of application

because the motor produces a high torque in a limited volume. In fact, its compactness makes the DC machine in a high level of saturation. However, this kind of machine comprises 4 or 6 poles in the stator. These poles are wide in comparison with synchronous machines where each pole is formed by many slots. Compared to this case, the impact of armature reaction is enhanced in our particular application. This phenomenon related to the rotor supply, generate a non-uniform flux density in the pole pitch from one side to the opposite one along the azimuthal direction. In the modeling of synchronous machine, some authors have neglected the AMR and others modeled it by a one simple reluctance. In our case, the AMR is highlighted due to the high saturation level in the same pole, which needs a special discretization of the pole. In this paper, the impact of modeling this phenomenon in the high saturated DC machine is highlighted.

The saturation is taken into account in the model through the $B(H)$ curve of the iron. The topology of the equivalent model is defined from the flux lines. This discretization is determined respecting the homogeneity of the flux density in ferromagnetic material. Indeed, the reluctance calculation of each flux tube is based on the assumption of a piecewise permeability factor, the following expression is used:

$$P(\varphi) = \int \frac{\mu_0 \, \mu_r(\varphi)}{l} \, dS \tag{1}$$

However, the airgap network reluctance should be determined precisely in order to model the right connections between the ferromagnetic elements of the stator and rotor. The airgap reluctances allow the transmission of the flux from the stator to the rotor. These connections define the saturation of the ferromagnetic reluctances in the boundary of the airgap. This key step determines the validity of the model. The magneto-motive force F of each element is the ratio of the flux φ to the permeance P of each flux tube (1):

$$F(\varphi) = \frac{\varphi}{P(\varphi)} = R(\varphi) \, \varphi \tag{2}$$

Each rotor slot is modeled by a set of reluctances R and a magneto-motive force F corresponding to the total ampere-turns in each slot. The AMR induces a high saturated level in a pole side and a low saturation in the opposite side due to the shifted stator and rotor magnetic fields. This phenomenon impacts the torque calculation when it is not considered. The AMR is modeled by both current sources in the rotor network and by tangential permeances (highlighted in red on Figure 1). The network corresponding to one stator pole is shown on the figure. It also contains the saturated reluctances of the iron paths (grey) and non saturated reluctances of air paths (blue) as classically adopted in electric machines equivalent networks.

To deal with this reluctance network containing a large number of nodes, a Kron reduction method applied to Kirchoff laws of electric circuits is used. The electric system of equations to be solved is:

$$[\mathbf{C}]^T \, [\mathbf{R}] \, [\mathbf{C}] \, [\boldsymbol{\varphi}] - [\mathbf{C}]^T \, [\mathbf{F}] = 0 \tag{3}$$

with:

- $[\mathbf{C}]$: the connection matrix,
- $[\mathbf{R}]$: the matrix of reluctances in different branches,
- $[\boldsymbol{\varphi}]$: the vector of flux of the main branches,

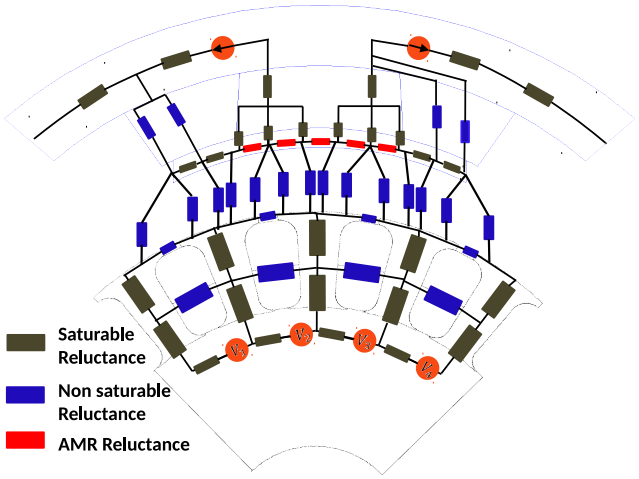

Figure 1. A portion of one pole RN model included AMR reluctances in the stator pole.

- [**F**]: the vector of MMFs of different branches.

In nonlinear conditions, it is necessary to apply an iterative method to reach the solution step by step. Some authors [14,19] use the Newton Raphson method that is usually applied with the finite element models. In our case, we choose a fixed point method for its robustness to converge which less depends on the chosen starting point. To accelerate the convergence, we can choose, into the permeability value, an optimized relaxation factor as can be seen in [15], or a simple fixed relaxation factor α as presented here. The convergence process is given by Algorithm 1. At the first iteration, all permeabilities are set to a fixed value that allows finding the first flux values. The flux density values are deduced and projected into the $B(H)$ curve which allows updating the value of the permeability of different reluctances. The process continues until the relative error between two successive values of the permeability does not exceed 1%.

Algorithm 1 Convergence process in nonlinear conditions

1: Initialization: $k = 1$, $\varepsilon_k = \infty$, $\mu_k = \mu_0$ { *permeabilities of each permeance* }
2: ***while*** $(\varepsilon_k > 1\%)$ ***do***
3: *Calculate the fluxes in each permeance* φ_{k+1}
4: *Deduce the equivalent flux densities* B_{k+1}
5: *Deduce the corresponding permeabilities from* $B(H)$ *curve* μ_{k+1} *and stock them in a vector* $[\boldsymbol{\mu_{k+1}}]$
6: $\varepsilon_{k+1} = \dfrac{\| [\boldsymbol{\mu_{k+1}}] - [\boldsymbol{\mu_k}] \|}{\| [\boldsymbol{\mu_k}] \|}$
7: $[\boldsymbol{\mu_{k+1}}] = [\boldsymbol{\mu_{k+1}}] + \alpha \cdot \left([\boldsymbol{\mu_k}] - [\boldsymbol{\mu_{k+1}}] \right)$
8: $k = k + 1$
9: ***end while***

2.2 Reducing CPU time by using an equivalent symmetrical machine

The studied machine has 4 poles in the stator ($N_s = 4$) and 19 rotor slots ($N_r = 19$). In the brushed DC machines, the simple wave winding requires an odd number of slots in the rotor to provide a balanced winding. Modeling this asymmetrical machine by a reluctance network requires establishing a network of the whole machine so that the number of degrees of freedom becomes very important and makes the resolution time consuming. An alternate way consists in considering a symmetrical equivalent machine and deals with one magnetic period and, therefore, reduces the size and simplifies the establishment of the reluctance network thanks to symmetry conditions. Therefore, the 4 poles-20 slots, 4 poles-18 slots machines are compared to choose the more convenient machine which can replaces the 4 poles-19 slots topology. On the Figure 2 the cross section of the three machines are shown.

A comparison of the instantaneous and average torque between two machines, with an even neighboring number of 19 rotor slots with the same stator pole number, and this referenced machine is shown in the Figure 3. The torque waveforms over one period are computed with 2D full finite element model. This comparison is focused on the average values and the ripple torque produced by these machines with the same total current in the rotor by keeping the same switching time. As it can be seen, the average torque produced by the machine of 4 poles-20 slots is slightly greater (4.7%), while the average torque of the 4 poles-18 slots machine is lower (16.5%) compared to the 4 poles-19 slots machine average torque. On the other hand, the ripple torque of the 18 slots machine is low, while the 20 slots machine torque ripple is higher. Indeed, the torque ripple period is calculated with the least common multiple (LCM) of the number of rotor slots and stator poles. The lower this common multiple is, the larger is the period of ripple, as expressed bellow by (4):

$$\tau_{\text{ripple}} = \frac{2\,\pi}{\text{LCM}(N_S, N_r)} \tag{4}$$

In terms of saturation level, the 20 slots machine and 18 slots machine are respectively more and less saturated than the reference machine. The 20 slot machine is a good equivalent machine which allows a good modeling of the saturation effect due to the rotor saliency. In this case, we can reduce the size of the reluctance network by modeling only half of the machine. In this equivalent machine, symme-

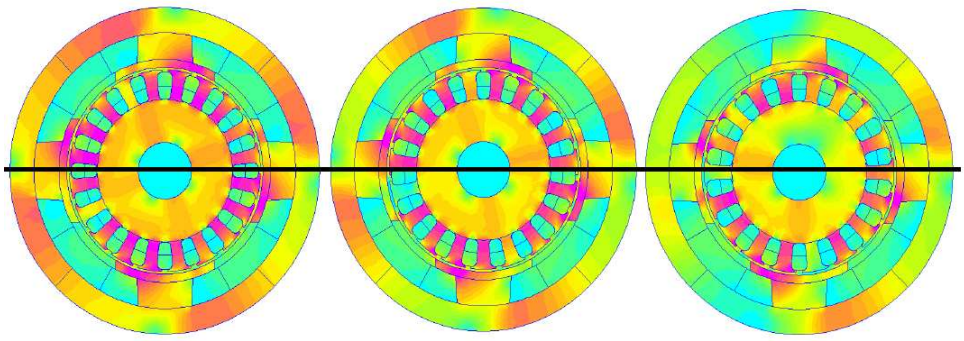

Figure 2. Cross sections of 4 poles-20 slots, 4 poles-19 slots, and 4 poles-18 slots machines.

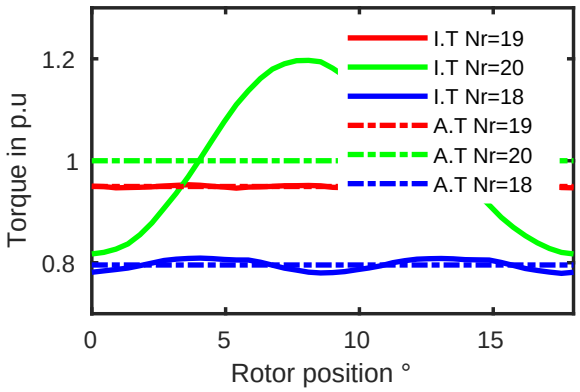

Figure 3. Comparison of torque curves between three different machines ($4\,p/19$ slots, $4\,p/20$ slots, $4\,p/18$ slots)

try of the flux lines and geometry are checked, the even harmonics are zero. Since the RN model allows to calculate the instantaneous torque value, the average value should be calculated using two calculations where the first one corresponding to the central position θ_0 and the second to the half period θ_1 of the ripple torque. The connections between the stator and the rotor through the airgap change between these two positions as can be seen in the Figure 4, two models of the airgap should be developed. Red and black reluctances correspond respectively to the position θ_0 and θ_1. Thus, the average torque T_{mean} can be calculated by using two positions shifted by half a period, using (5) and (6):

$$T_{\text{mean}} = \frac{T(\theta_0) + T(\theta_1)}{2} \tag{5}$$

$$\theta_1 = \theta_0 + \frac{\tau_{\text{ripple}}}{2} \tag{6}$$

where:

- θ_0 is the central position of the rotor,
- θ_1 is the shifted position of the rotor.

2.3 Validation of the model

2.3.1 Validation using several operating points The torque values given by the RN and 2D finite element models are compared in the same conditions. Indeed, once the circuit equation is solved, the flux φ_k, the magneto-motive force F_k and the coenergy $\widetilde{W_k}$ in each branch are known. Hence:

$$\widetilde{W_k}\big(\theta, F_k(I)\big) = \int_0^{F_k(I)} \varphi_k(\theta, F)\, dF = \int_0^{F_k(I)} P_k(\theta, F)\, F\, dF \tag{7}$$

The total coenergy $\widetilde{W}$ is the sum of these elementary coenergies:

$$\widetilde{W}(\theta, I) = \sum_{k=1}^{N} \widetilde{W_k}\big(\theta, F_k(I)\big) \tag{8}$$

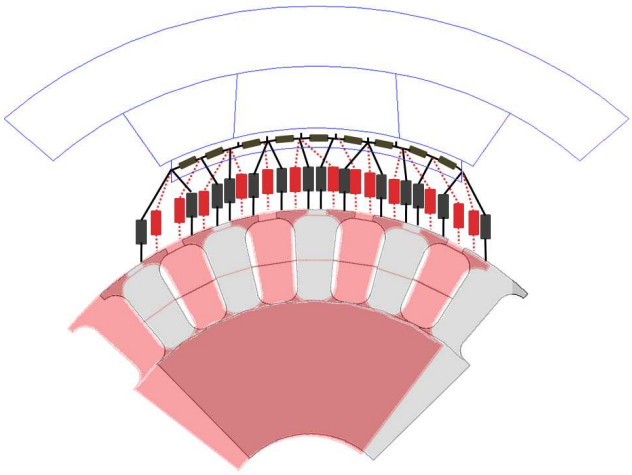

Figure 4. Change of the air-gap network between θ_0 (red RN) and θ_1 (grey RN) rotor positions

The torque is then calculated from the variation of the coenergy $\delta\widetilde{W}$ around each position by making a slight displacement on the rotor position $\delta\theta$. It comes (9):

$$T(\theta, I) = \frac{\delta\,\widetilde{W}(\theta, I)}{\delta\theta} \tag{9}$$

The torque is calculated for both θ_0 and θ_1 positions to obtain the average value. A comparison between the coenergy obtained by the RN model and by 2D FE in both rotor positions θ_0 and θ_1 for different current values is presented in the Figure 5(a). A good agreement is observed even in saturated conditions. The torque corresponds to the variation of the coenergy, then the good agreement on the coenergy leads to the good agreement on the torque displayed in Figure 5(b).

On Figure 6(a), the average torque obtained by the average value given from Figure 5(b) (blue curve) is compared to results computed by 2D and 3D finite element (red curves). In addition experimental results (black curve) are added on this figure to show the effectiveness of the modeling accounting for armature reaction. Again, a really good agreement between these models is observed.

In this section, we can also illustrate how much important the magnetic armature reaction can be when it is neglected in the reluctance network due to the high saturated operation DC starter. Indeed, in Figure 6(a), the green curve represents the torque-current curve given by the RN without considering the AMR tangential reluctance in the pole shoe. This green curve gives a bad torque evaluation due to the absence of the tangential reluctances. This hypothesis gives a wrong flux density distribution under the pole shoe. The tangential reluctances allow the modelling of the tangential path of the armature reaction flux and lead to a better modelling of this physical phenomenon in this key part of the machine. In the Figure 6(b), the level of the flux density in the pole shoe overtake the 2 T value while in all other part of the machine it is under 2 T.

2.3.2 Validation by a statistical approach Before using this model in an optimization process, another way to validate its robustness consists on a statistical

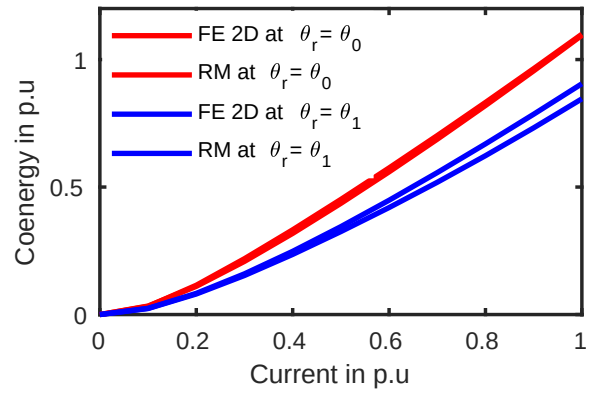

(a)

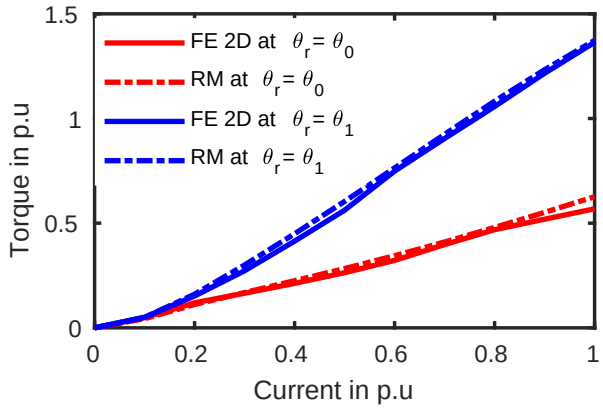

(b)

Figure 5. (a): Comparison of the coenergy-current's curves between 2D FE and RN in both rotor positions; (b): Comparison of the Torque-current's curves between 2D FE and RN in both rotor positions.

approach based on 1000 random machines. The main goal is to reach the better geometrical parameters for a given topology. In this case, the number of stator poles and rotor slots are kept constant. To randomize these machines, several geometrical parameters shown in the Figure 7(a) are chosen in a specific range which corresponds to the domain D as provided by Table 1. For each random machine, the average torque is calculated using the two RN models and the two corresponding computations by 2D FE. The obtained relative error is then presented in the Figure 7(b). A Gaussian distribution allows to conclude that the model presents about 700 among 1000 machines with a relative error under $\pm 5\%$. The average of this Gaussian is located at -5% with a variance of 0.0027, the relative error between finite elements and our model for 95% of the tested machines is located between $[-15\%, +5\%]$.

The optimization of the machine requires a saving time model, we compared the CPU time between the model and 2D and 3D finite element regarding the number of nodes in each model. These calculations are performed on an Intel Xeon E5-2609

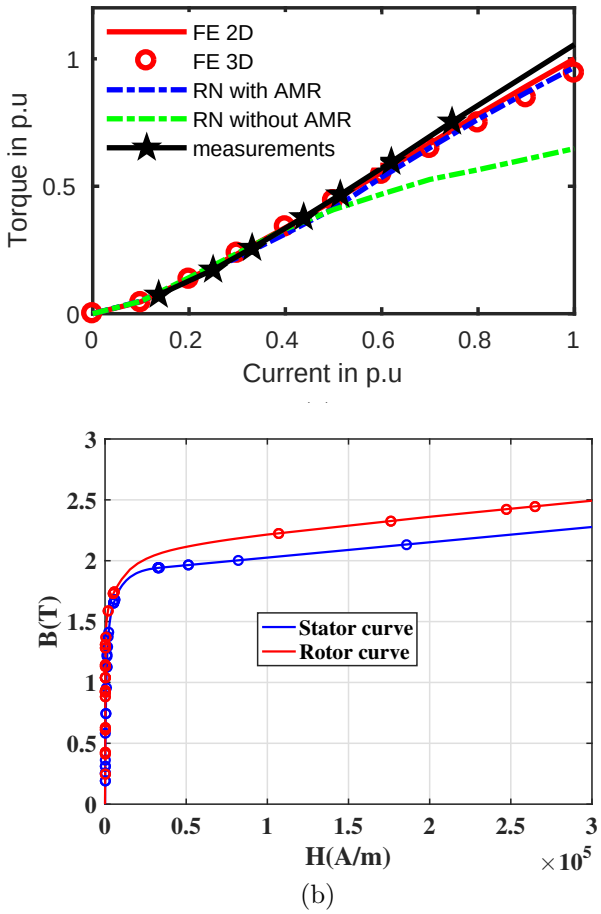

(b)

Figure 6. (a): Torque-current curves with RN with and without AMR reluctances compared to 2D/3D FE and measurements; (b): Flux density of each element in the RN corresponding to the current=1 p.u projected in B(H) curve.

@2.4 GHz processor. As presented in Table 2, the model provides an advantageous time calculation with 3.6 seconds compared to 2D FE with 112 seconds and 3D FE with 27 minutes for the calculation of one operating point.

Then our model is particularly suitable for optimization purpose. However the optimization is considered the best means to test the robustness of the RN model since, generally, errors due to simplification hypotheses are emphasized during an optimization process.

3 Inclusion in an optimization process

The RN model developed here is enough accurate and robust with low time calculation and suitable for an optimization use. The main objective is to use the RN model to optimize the machine regarding the lifetime, compactness. The lifetime of the DC machine in our application is directly linked to brush wear due to the speed, our goal is then increasing the torque T_m of the machine making the speed

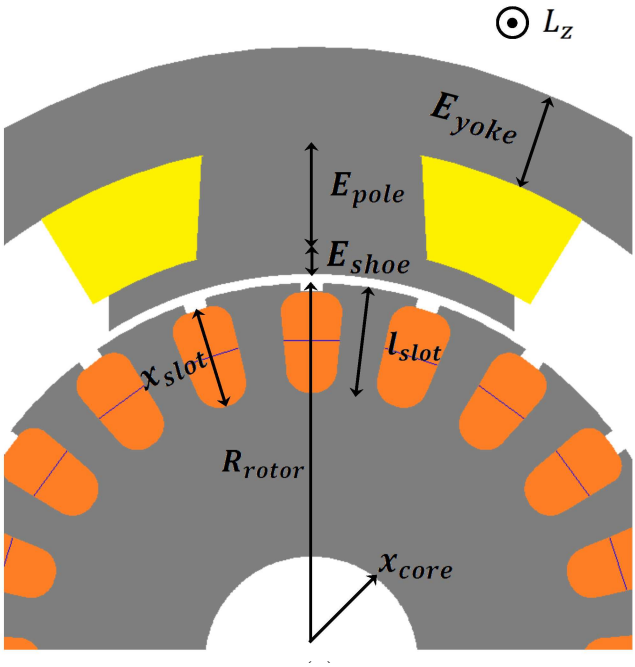

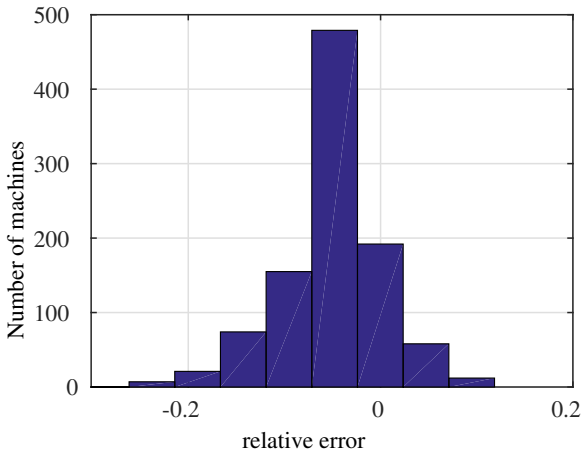

(b)

Figure 7. (a): Geometrical parameters of the machine used for statistical validation and optimization; (b): Gaussian distribution of the relative error between FE and RN based on 1000 random machines.

decreasing. However, losses in machine can be decreasing, in our application the main losses are due to the copper losses than can be decreasing here by decreasing the winding resistance, otherwise the resistance limit the voltage battery drop. Then the resistance will be kept constant in our optimization, thanks to the equality constraint: $R(\mathbf{x}) = R_{ref}$. Furthermore, the constraint related to the resistance due to the starter supply with a 12V battery limits copper losses which reduces the temperature rise of the starter. The temperature variation are not considered due

Table 1
Variation range of each geometrical parameter in D domain

Variable parameters	Unit	Domain D
R_{rotor}	mm	$[22.5, 27.5]$
x_{core}	%	$[15, 40]$
l_{slot}	mm	$[6, 11]$
x_{slot}	%	$[75, 96]$
E_{pole}	mm	$[5.5, 10]$
E_{yoke}	mm	$[3, 13]$
L_z	mm	$[20, 45]$

Table 2
Comparison of CPU time of the three different magnetic models

	Number of nodes	CPU time
3D FE	180233	27 min
2D FE	37500	112 s
RN	59	3.6 s

to the very fast transient operation of such devices. The compactness is respected by limiting the external volume of the machine. We aim to increase the torque of the machine respecting the sizing limitation by keeping the resistance constant. In the following, an optimization, mixing a global stochastic algorithm and a local deterministic one, is performed for a mono-objective problem and compared to a multi-objective problem using a meta-heuristic algorithm.

3.1 Mono-objective problem

In this section, the final goal is to get one optimized machine using a local deterministic algorithm based on a Sequential Quadratic Programming (SQP), but for this step an initial machine is needed. A meta-heuristic algorithm which is a classical particle swarm optimization (PSO) [24] is used for 1000 evaluations of the objective function with 20 particles moving during 50 iterations. The same geometrical parameters as in the statistical way were chosen for this optimization evolving with the same variation range (domain D).

The optimization problem used is written as follow:

$$\begin{cases} \max\limits_{\mathbf{x} \in D} T_m(\mathbf{x}) \\ \text{with: } \mathbf{x} = (R_{\text{rotor}}, x_{\text{core}}, l_{\text{slot}}, E_{\text{pole}}, E_{\text{yoke}}, L_z) \\ \text{subjected to: } \begin{cases} V_{\text{ext}}(\mathbf{x}) \leq V_{ref} \\ R(\mathbf{x}) = R_{ref} \end{cases} \end{cases} \tag{10}$$

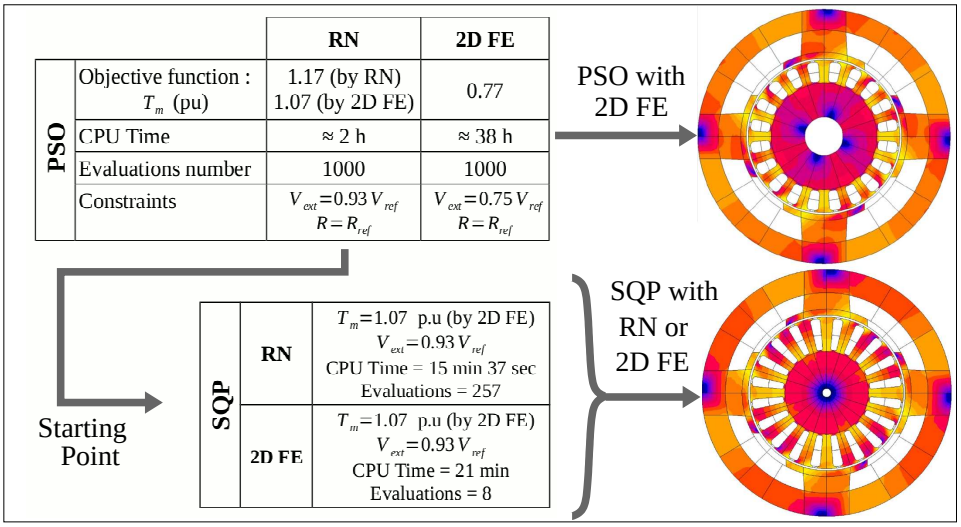

Figure 8. First optimization example using PSO and SQP with RN and FE models

The optimization using a PSO was used on both the reluctance network and the 2D finite element. Then, we can use four different methods to solve our problem:

- Method #1: only PSO algorithm associated to RN,
- Method #2: only PSO algorithm associated to 2D FE,
- Method #3: use Method# 1 to obtain a preliminary solution $\mathbf{x_0}$ which is used as a starting point for a SQP algorithm also associated to RN,
- Method #4: same as Method #3 but with SQP associated with 2D FE.

Method #1 is applied first. After 2 hours computation using reluctance model an improved machine is obtained. This machine was checked by 2D FE and provides a higher torque (7%) and respects the volume limit. Concerning the method #2, after 38 hours of computation using the 2D finite element in the same optimization process, we conclude that the FE was limited to a bad machine with a lower torque (23%). Results are given by Figure 8.

For Methods #3 and #4: the initial solution provided by the PSO using the RN (with 7% higher torque) is used as a starting point $\mathbf{x_0}$ in a SQP optimization process dealing with the same problem formulation. Both models were compared again. It seems that the solution obtained by RN model after 257 evaluations during 15 min, and the one obtained by 2D FE after 8 evaluations during 21 min are exactly the same than the starting point $\mathbf{x_0}$. Then, we can conclude that this solution, which is the optimized machine using PSO and the RN model in the first step, surely corresponds to the global minimum of our problem. Through this practical case, we can conclude that Method #1 is enough efficient for solving our mono-objective design problems since the best machine was directly obtained by a PSO using the RN model in 2 hours. Moreover, it proves the interest of the developed RN model.

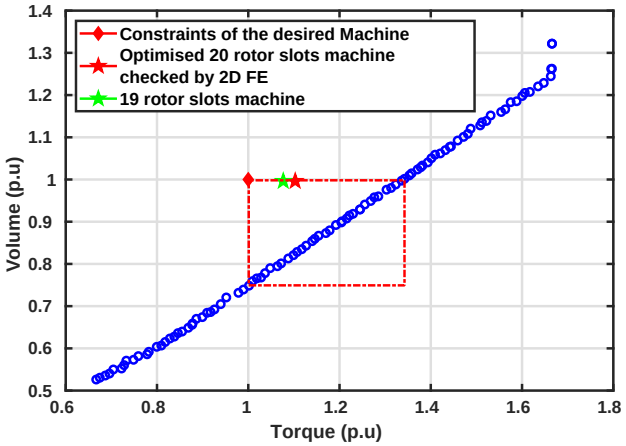

Figure 9. Pareto front using NSGAII with RN model, 4 pole-20 slot and 4 pole-19 slot machines checked with FE

3.2 Multi-objective problem

An other way consists in looking for many solutions or machines that satisfy the problem constraints. A meta-heuristic multi-objective Non-dominated Sorting Genetic Algorithm (NSGA II) is performed to build a relevant Pareto front. It allows us to see the evolution of machine in a specific range according to the torque and volume specifications and getting many different machines respecting the optimization criteria. Using by the NSGA, the main objectives are maximizing the torque while minimizing the machine volume, while respecting that the resistance R must be equal to a fixed value R_{ref}.

The problem is then formulated as follow:

$$\begin{cases} \left(\max\limits_{\mathbf{x} \in D} T_m(\mathbf{x}) \ , \ \min\limits_{\mathbf{x} \in D} V_{\text{ext}}(\mathbf{x}) \right) \\ \text{with:} \ \ \mathbf{x} = (R_{\text{rotor}}, x_{\text{core}}, l_{\text{slot}}, E_{\text{pole}}, E_{\text{yoke}}, L_z) \\ \text{subjected to:} \ \ R(\mathbf{x}) = R_{ref} \end{cases} \tag{11}$$

Several optimized machines have shaped the Pareto front using only the reluctance model with the NSGA algorithm (Figure 9). The interesting area is located in $V_{\text{ext}} \leq 1$ p.u and $T_m \geq 1$ p.u. (red rectangle on the figure). In this area, one random machine was checked by FE, and a slightly difference between the results given by the model and 2D finite element can be shown. This difference corresponds to the black arrow plot on the figure (between a blue point of the front and the real value represented by the red star).

This 4 pole-20 slot optimized machine presents a higher torque (compared to our reference, the red diamond). The real desired machine have 19 slots. Then, the 4 pole-19 slot machine corresponding to our solution is checked by 2D FE. It presents 7% higher torque than the initial starter with the same volume. This final optimized machine is shown by Figure 10.

The mono-objective optimization using a mixing approach PSO+SQP or only PSO and the multi-objective optimization using a meta-heuristic NSGA gives two

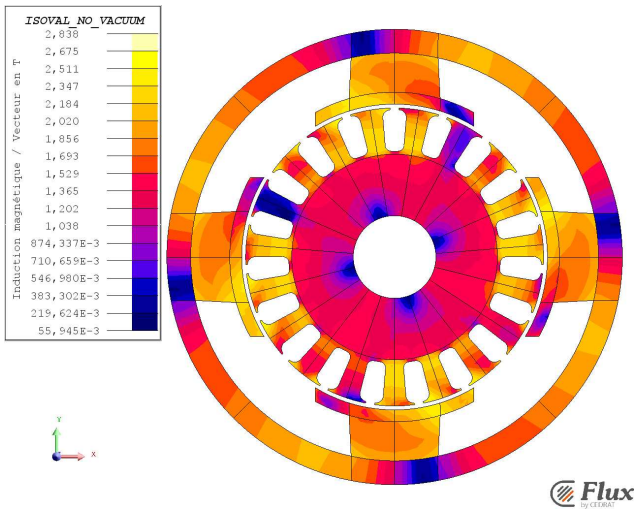

Figure 10. The 4 pole-19 slot optimized machine checked by 2D FE and flux density distribution for current=1 p.u

different better machines than the initial existing starter thanks to the developed reluctance network. While the machine given by the mono-objective method presents a thick yoke and a deep slots, the machine given by NSGA II presents a thin yoke and a shallower slots. But both have some real interests.

4 Conclusion

In this paper, a reluctance network model is developed with the consideration of armature reaction magnetic in a high saturated machine. The effect of taking into account the armature reaction due to the rotor current by adding tangential reluctances in the stator pole on the torque calculation is highlighted. Then the model presents a good agreement with 2D and 3D finite element computations for many operating points in terms of torque calculation. This model presents also a good robustness as shown by a statistical validation made on a 1000 randomized machines. Thanks to its reduced CPU time, two examples of optimization are performed. The first consists in using a mono-objective stochastic PSO algorithm to reach a first solution used as starting point in a mono-objective local deterministic SQP. Both algorithms are also applied using 2D FE. Comparing the solutions shows the possibility to optimize directly the machine using only a PSO associated to the developed RN. A second design example is carried out using the RN model associated with a NSGA II algorithm for solving a multi-objective problem. Several machines better than the initial one are obtained. These examples show the efficiency of the RN model to find a good optimum. This model could also be used with an electrical model to study the influence of the saturation on the commutation or to optimize the machine in dynamic cycles. This will be done in a future work.

References

[1] Andreux, R., Fontchastagner, J., Takorabet, N., Labbe, N. and Metral, J.-S., "A general approach for brushed DC machines simulation using a dedicated field/circuit coupled method," *PIER*, Vol. 145, 213–217, 2014.

[2] Vauquelin, A., Vilain, J.-P., Vivier, S., Labbe, N. and Dupeux, B., "A new modeling of DC machine taking into account commutation effects," *Proc. XVIII International Conference on Electrical Machines (ICEM'2008)*, Villamoura, Portugal, Sept. 6–9, 2008.

[3] Andreux, R., Fontchastagner, J., Takorabet, N. and Labbe, N., "A Fast Finite Element Model Taking Into Account 3-D Effects for the Optimal Design of Micro-Hybrid Starters," *IEEE Trans. Magn.*, Vol. 50, No. 5, 1–8, 2014.

[4] Fassenet, M., Pera, T., Chamagne, D. and Kauffmann, J. M., "Optimal Design of Small Power DC PM Commutator Motors, Part I: Analytic Model," *Electr. Power Compon. Syst.*, Vol. 32, No. 10, 2004.

[5] Fassenet, M., Pera, T., Chamagne, D. and Kauffmann, J. M., "Optimal Design of Small Power DC PM Commutator Motors, , Part II: Implementation and Results of the Optimization Procedure," *Electr. Power Compon. Syst.*, Vol. 32, No. 10, 2004.

[6] Mahmoudi, A., Rahim, N.A. and Ping, H.W., "Genetic algorithm and finite element analysis for optimum design of slotted torus axial-flux permanent-magnet brushless DC motor," *PIER B*, Vol. 33, 383–407, 2011.

[7] Lubin, T., Mezani, S. and Rezzoug, A., "Improved analytical model for surface-mounted pm motors considering slotting effects and armature reaction," *PIER B*, Vol. 25, 293–314, 2010.

[8] Liu, X., Hu, H., Zhao, J., Belahcen, A. and Tang, L., "Armature Reaction Field and Inductance Calculation of Ironless BLDC Motor," *IEEE Trans. Magn.*, Vol. 52, No. 2, 1–14, 2016.

[9] Ostovic, V., "Magnetic equivalent circuit presentation of electrical machines," *Electr. Mach. Power Syst.*, Vol. 12, No. 6, 1987.

[10] Ostovic, V., Miller, J. M., Garg, V. K., Schultz, R. D. and Swales, S. H., "A magnetic-equivalent-circuit-based performance computation of a Lundell alternator," *IEEE Trans. Ind. App.*, Vol. 35, No. 4, 825–830, 1999.

[11] Li, W. and Huang. S., "Analysis and Design of Hybrid Excitation Claw-pole Generator," *Electr. Power Compon. Syst.*, Vol. 39, No. 7, 2011.

[12] Hecquet, M. and Brochet, P., "Modeling of a claw-pole alternator using permeance network coupled with electric circuits," *IEEE Trans. Magn.*, Vol. 31, No. 3, 2131–2134, 1995.

[13] Ibala, A., Rehbi, R. and Masmoudi, A., "Magnetic equivalent circuit based modeling of claw pole machines : A survey," *Electrical Machines and Systems (ICEMS), 2011 International Conference on*, 1–6, Aug. 20-23, 2011.

[14] Asghari, B. and Dinavahi, H., "Novel Transmission Line Modeling Method for Nonlinear Permeance Network Based Simulation of Induction Machines," *IEEE Trans. Magn.*, Vol. 47, No. 8, 2100–2108, 2011.

[15] Guo, Y.G., Zhu, J.G. and Lu, H.Y., "Effects of Armature Reaction on the Performance of a Claw Pole Motor With Soft Magnetic Composite Stator by Finite-Element Analysis," *IEEE Trans. Magn.*, Vol. 43, No. 3, 1072–1077, 2007.

[16] Zhang, Z., Sun, L., Tao., Y. and Yan, Y., "Development of nonlinear magnetic network model of a hybrid excitation doubly salient machine," *Electrical Machines and Drives (IEMDC), 2013 International Conference on*, 663–669, May 12-15, 2013.

[17] Belalahy, C., Rasoanarivo, I. and Sargos, F.M., "Using 3D reluctance network for design a three phase synchronous homopolar machine," *Industrial Electronics (IECON), 2008 International Conference on*, 2067–2072, Nov. 10-13, 2008.

[18] Hua, W., Zhang, G., Cheng, M. and Dong, J., "Electromagnetic Performance Analysis of Hybrid-Excited Flux-Switching Machines by a Nonlinear Magnetic Network Model," *IEEE Trans. Magn.*, Vol. 47, No. 10, 3216–3219, 2011.

[19] Yu, Q., Wang, X. and Cheng, Y., "Magnetic Modeling of Saliency Effect for Saturated Electrical Machines with a New Calculation Method," *IEEE Trans. Magn.*, Vol. 52, No. 6, Article#: 8001106, 2011.

[20] Amrhein, M. and Krein, P. T., "3-D Magnetic Equivalent Circuit Framework for Modeling Electromechanical Devices," *IEEE Trans. Energy Convers.* , vol. 24, no. 2, pp. 397-405, June 2009.

[21] Andreux, R., Fontchastagner, J., Takorabet, N., Labbe, N. and Metral, J.-S., "Magnetic field-electric circuit coupled method for brush DC motor simulations," *Electrical Machines (ICEM), 2012 XXth International Conference on*, 2683–2688, Sept. 2-5, 2012.

[22] Li, L., Foggia, A., Kedous-Lebouc, A., Mipo, J.C. and Kobylansky, L., "Some armature reaction compensation methods numerical design of experiments and optimization for a hybrid excitation machine," *Electrical Machines and Drives (IEMDC), 2009 International Conference on*, 832–838, May 3-6, 2009.

[23] Nguyen-Xuan, H., Dogan, H., Perez, H., Gerbaud, S., Garbuio, L. and Wurtz, F., "Efficient Reluctance Network Formulation for Electrical Machine Design Using Optimization," *IEEE Trans. Magn.*, Vol. 50, No. 2, 869–872, 2014.

[24] Alrashidi, M. R. and El-Hawary, M. E., "A Survey of Particle Swarm Optimization Applications in Power System Operations,", *Electr. Power Compon. Syst.*, Vol. 34, No. 12, 2006.